Kobe University Repository : Kernel

PDF issue: 2026-10-30

Effect of molecular structure on porous structure and performance of star-branched poly(lactic acid) ultrafiltration membranes

Takada, Koichi ; Okada, Akinori ; Hirano, Hiroshi ; Kadota, Joji ; Kitagawa, Tooru ; Matsuyama, Hideto ; Yoshioka, Tomohisa ; Nakagawa,…

(Citation)
Journal of Membrane Science,744:125225

(Issue Date)
2026-04

(Resource Type)
journal article

(Version)
Version of Record

(Rights)
© 2026 The Authors. Published by Elsevier B.V.
This is an open access article under the Creative Commons Attribution-NonCommercial-NoDerivatives 4.0 International license

(URL)
https://hdl.handle.net/20.500.14094/0100501332

Journal of Membrane Science 744 (2026) 125225

Contents lists available at ScienceDirect

Journal of Membrane Science

journal homepage: www.elsevier.com/locate/memsci

Effect of molecular structure on porous structure and performance of star-branched poly(lactic acid) ultrafiltration membranes

Koichi Takada [a,b,*], Akinori Okada [a], Hiroshi Hirano [a], Joji Kadota [a], Tooru Kitagawa [b,c], Hideto Matsuyama [c,d], Tomohisa Yoshioka [b,c], Keizo Nakagawa [b,c,**]

[a] Research Division of Materials Science and Engineering, Osaka Research Institute of Industrial Science and Technology, 1-6-50, Morinomiya, Joto, Osaka, 536-8553, Japan
[b] Graduate School of Science, Technology, and Innovation, Kobe University, 1-1 Rokkodai, Nada, Kobe, 657-8501, Japan
[c] Research Center for Membrane and Film Technology, Kobe University, 1-1 Rokkodai, Nada, Kobe, 657-8501, Japan
[d] Department of Chemical Science and Engineering, Kobe University, 1-1 Rokkodai, Nada, Kobe, 657-8501, Japan

ARTICLE INFO

Keywords:
Poly(lactic acid)
Branched structure
Ultrafiltration membrane
Nonsolvent-induced phase separation
Biodegradable polymer

ABSTRACT

Poly(lactic acid) (PLA) is a biomass-derived biodegradable polymer that shows promise as a circular resource for water-treatment membranes. The molecular structure of PLA affects its phase separation behavior, enabling control of pore formation to improve membrane performance. Changing the molecular chain density of PLA also affects its biodegradation behavior. However, conventional polymerization methods hardly provide PLA with both narrow molecular-weight distribution and high molecular weight, which limits research on the molecular structure of PLA. In this study, linear and star-branched PLA with four or eight arms were synthesized via organocatalyzed ring-opening polymerization, achieving a weight-average molecular weight (M_w) of ~95,000 and narrow dispersity ($\leq$1.2). PLA membranes were prepared via nonsolvent-induced phase separation and the effects of branch number and M_w on pore structure and hydrolysis behavior were investigated. The membrane surfaces exhibited fine pores with underlying finger-like macrovoids. Molecular weight cut-off increased with branch number (linear: 15,000 Da; four: 17,000 Da; eight: 52,000 Da). This trend was attributed to the decrease in solution viscosity with increasing branch number, which facilitated phase separation and pore growth. The decrease rate of molecular weight in accelerated hydrolysis tests (pH 9, 65 °C, 215 h) was 90 % for four-arm PLA, 70 % for linear, and 49 % for eight-arm PLA. A moderate PLA branching structure promoted hydrolysis, whereas an excessive branch number increased the chain density near the branch points, inhibiting water penetration and hydrolysis. These findings indicate that branch number, M_w, and viscosity control are important for improving membrane performance and degradability.

1. Introduction

Ultrafiltration (UF) membranes are widely used because of their low energy consumption, compact system footprint, and high reliability in terms of product purity compared with the performance of other conventional separation methods. Materials used for membranes are often petroleum-derived and non-biodegradable polymers such as polyethylene [1,2], polysulfone [3,4], and poly(vinylidene fluoride) [5,6]. UF and microfiltration (MF) membranes composed of these materials are used for drinking water treatment, wastewater treatment, industrial water purification, and in food and beverage industries [7]. Biomass-derived and/or biodegradable polymers are favorable materials for limiting carbon dioxide emissions and preventing waste from remaining in the environment. Representative examples include poly (butylene succinate) (PBS), poly(3-hydroxybutyrate-co-3-hydroxy hexanoate), and poly(lactic acid) (PLA), the latter of which has achieved the most extensive industrial application [8]. PLA is a circular resource-type material that does not biodegrade in water at ordinary temperatures, which makes it promising for use in water-treatment membranes [7]. PLA MF and UF membranes prepared via phase

* Corresponding author. Research Division of Materials Science and Engineering, Osaka Research Institute of Industrial Science and Technology, 1-6-50, Morinomiya, Joto, Osaka, 536-8553, Japan.
** Corresponding author. Graduate School of Science, Technology, and Innovation, Kobe University, 1-1 Rokkodai, Nada, Kobe, 657-8501, Japan.
E-mail addresses: takada.koichi@orist.jp (K. Takada), k.nakagawa@port.kobe-u.ac.jp (K. Nakagawa).

https://doi.org/10.1016/j.memsci.2026.125225
Received 25 November 2025; Received in revised form 20 January 2026; Accepted 28 January 2026
Available online 29 January 2026
0376-7388/© 2026 The Authors. Published by Elsevier B.V. This is an open access article under the CC BY-NC-ND license (http://creativecommons.org/licenses/by-nc-nd/4.0/).

separation have been reported. For example, Tanaka et al. demonstrated PLA MF membranes with bacterial removal capability and investigated how the preparation process influenced membrane structure and performance [9–11]. Moriya and colleagues reported hollow-fiber PLA UF membranes, in which the addition of polyethylene glycol (PEG)–PLA copolymers imparted antifouling properties [12,13]. Other studies highlighted the effects of coagulation bath composition and the PLA concentration of casting solution on membrane structure [14,15].

In the development of PLA-based membranes, two major points need to be considered: molecular structure and biodegradability. The molecular structure of PLA controls membrane structure and performance. However, previous studies have been limited to stereocomplex PLA, which is composed of D- and L-enantiomers [16,17], or copolymers of PLA with other polymers [18]. In addition, PLAs used in previous studies have been linear; the effect of a branched structure on phase separation structure has not been investigated. The reasons are follows: 1. commercially available PLA only has linear molecular structure; PLA with controlled molecular structures is not available; 2. conventional tin-based catalysts commonly used for PLA synthesis tend to induce side reactions that generate linear chains, making it difficult to obtain branched PLA with high purity; 3. the side reactions broaden molecular weight distribution [19].These reasons make it difficult to distinguish the effects of molecular weight and branch structure on phase separation structure. Although catalysts that suppress side reactions have been reported [20,21], the molecular weights achieved are generally around 10,000, which is insufficient to impart the mechanical strength required for the porous structures of membranes.

Biodegradation of PLA membranes is another consideration. Conventional linear PLA typically takes a long time to degrade, and thus accelerating its decomposition after use is desirable. PLA degradation proceeds in two stages: initial chemical hydrolysis, which decreases molecular weight, followed by microbial assimilation once the arm chain length of PLA decreases to below about 10,000 Da [22,23]. The initial hydrolysis strongly accelerates above the glass transition temperature (T_g), yet even then, substantial time is required before the onset of microbial degradation. Although copolymerization with other biodegradable monomers has been investigated to address this issue, it often results in an undesirable decrease of T_g because many biodegradable polymers exhibit low T_g [24]. PLA has a T_g of 50–60 °C, and thus hydrolysis does not progress easily under general water-treatment conditions (below 40 °C). However, if copolymerization decreases T_g below the operating temperature, there is a risk accelerating undesired degradation during use. Introducing a branched structure into PLA has been proposed as a strategy to accelerate degradation. This approach does not decrease T_g [25,26], and therefore it is considered that branched PLA will be suitable for use in water-treatment membranes.

Our research group has developed an organocatalyst capable of suppressing side reactions, enabling the synthesis of star-branched PLA with high molecular weight and narrow molecular weight distribution [27,28]. These PLAs possess the strength required for use as membranes because of their high molecular weight and make it possible to investigate the relationship between molecular structure (e.g., branch number) or molecular weight and membrane structure. In this study, we examine how the primary structure of PLA (molecular structure or molecular weight) affects its pore structure (phase separation structure). Linear and star-branched PLAs with different branch number and molecular weight are synthesized by ring-opening polymerization of lactide. Then, membranes are prepared via nonsolvent-induced phase separation (NIPS). Membrane structure and performance are evaluated to investigate their relationship with the primary structure of PLA. Four-arm star-branched PLAs with different molecular weight are studied to investigate the effect of molecular weight on membrane structure and performance. Hydrolysis of these membranes is investigated by measuring the time-dependent change of molecular weight in accelerated hydrolysis tests. The relationship between molecular structure and hydrolysis behavior is analyzed. This investigation covers not only the production and use of PLA UF membranes but also their disposal to assess their environmental impact after use.

2. Experimental section

2.1. Materials

L-Lactide (L-LA), pentaerythritol (PeOH), N,N′-diisopropylcarbodiimide (DIPCI), *p*-toluenesulfonic acid, lithium bromide (LiBr), and sodium azide (NaN_3) were purchased from Tokyo Chemical Industry (Tokyo, Japan). 4-Dimethylaminopyridine (DMAP), dichloromethane (CH_2Cl_2; stabilized with 2-methyl-2-butene), tetrahydrofuran (THF; stabilized with 2,6-di-*t*-butyl-4-methylphenol), deuterated chloroform ($CDCl_3$; stabilized with silver foil and 0.003 % tetramethylsilane), PEG 600, and PEG 6000 were purchased from Nacalai Tesque, Inc. (Kyoto, Japan). L-Lactic acid, ethylene glycol, molecular sieves 3A, molecular sieves 4A, 1-methyl-2-pyrrolidone (NMP), N,N-dimethylformamide (DMF), sodium nitrate ($NaNO_3$), and PEG 100,000 were purchased from Fujifilm Wako Pure Chemical Corporation (Osaka, Japan). Trifluoromethanesulfonic acid (TfOH), tripentaerythritol (TriPeOH), PEG 10,000, PEG 20,000, and PEG 35,000 were purchased from Sigma-Aldrich Japan (Tokyo, Japan). Easi Vial PEG/PEO was purchased from Agilent Technologies, Inc. (Santa Clara, CA, USA). L-LA was recrystallized three times from toluene and stored under nitrogen at 4 °C. DMAP was purified by sublimation and stored under nitrogen. All other materials were used as received.

2.2. Ring-opening polymerization of L-LA

Linear PLA with hydroxyl groups at both ends (HO-PLA-OH), linear PLA with a carboxylic acid group at one end and hydroxyl group at the other end (HOOC-PLA-OH), and star-branched PLA were synthesized in accordance with previously reported methods [27,28]. In this paper, four-arm star-branched PLA with a weight-average molecular weight (M_w) of 100,000 is designated as 4S-PLA-100k according to its branch number and M_w.

A typical polymerization procedure was conducted as follows. A 20-mL Schlenk flask was flame-dried under vacuum and then DMAP (1 mol%), 4-dimethylaminopyridinium trifluoromethanesulfonate (DMAP·HOTf; 1 mol%), L-LA (10 mmol), and initiator alcohol (0.07–0.50 mmol) were successively added. The mixture was stirred under nitrogen at 110 °C for 45–120 min (detail conditions are shown in Table 1). The reaction product was dissolved in CH_2Cl_2 (7 mL). The resulting solution was added dropwise into cold methanol (300 mL) to give a white precipitate. The obtained crude polymer was dried under vacuum at 40 °C for 5 h.

To purify the crude polymer to obtain star-branched PLAs (4S-PLA-50k, 4S-PLA-65k, 4S-PLA-100k, and 8S-PLA-100k), it was dissolved in THF and then methanol was slowly added dropwise until a precipitate formed. The fractions with high molecular weight were collected and then dried under vacuum at 40 °C for 6 h before use in subsequent experiments.

2.3. Synthesis of L-PLA-100k by condensation of HO-PLA-OH and HOOC-PLA-OH

The synthesis of linear PLA with M_w of ~100,000 (L-PLA-100k) was conducted as follows. A 50-mL screw-top test tube was flame-dried and then DMAP (0.035 mmol), 4-dimethylaminopyridinium *p*-toluene sulfonate (DMAP·HOTs; 0.035 mmol), HO-PLA-OH (0.01 mmol), HOOC-PLA-OH (0.015 mmol), CH_2Cl_2 (dehydrated with molecular sieves 3A, 2.8 mL), and 3A and 4A molecular sieves were successively added. The mixture was stirred at room temperature for 2 h. DIPCI (0.071 mmol) was added and then the mixture was stirred at 30 °C for16 h. After dilution with CH_2Cl_2 (1 mL), the solution was filtered through a polytetrafluoroethylene syringe filter (0.2-μm pore diameter) and then

Table 1
Polymerization conditions, number-average molecular weight (M_n), weight-average molecular weight (M_w), and dispersity (M_w/M_n) of PLAs.

Run	Sample	Initiator			Time	M_n	M_w	M_w/M_n
		Alcohol	Branch number	mol%	[min.]	[−]	[−]	[−]
1	HO-PLA-OH	Ethylene glycol	–	0.50	120	42,200	52,700	1.25
2	HOOC-PLA-OH	l-lactic acid	–	0.07	90	19,100	27,000	1.42
3	L-PLA-100k	–	–	–	–	81,400	97,300	1.20
4	4S-PLA-100k	Pentaerythritol	4	0.07	120	81,300	95,800	1.18
5	8S-PLA-100k	Tripentaerythritol	8	0.20	90	87,000	94,500	1.09
6	4S-PLA-65k	Pentaerythritol	4	0.07	50	62,000	65,900	1.06
7	4S-PLA-50k	Pentaerythritol	4	0.20	45	48,100	50,000	1.04

added dropwise into cold methanol to obtain a white precipitate. The precipitate was dried under vacuum at 40 °C for 5 h. The precipitate (475 mg) was dissolved in THF (25 mL) and then methanol (2.3 mL) was added dropwise. The precipitated fraction with high molecular weight was collected and then dried under vacuum at 40 °C for 6 h to give L-PLA-100k.

2.4. Polymer characterization

The obtained products were analyzed by ^{1}H nuclear magnetic resonance (NMR) spectroscopy (400 MHz, JNM-ECZ400R, JEOL Ltd., Japan) using $CDCl_3$ as the solvent. The number-average molecular weight (M_n), M_w, and dispersity (M_w/M_n) of PLA were determined by gel permeation chromatography (GPC). Absolute molecular weight was measured by a high-performance GPC system (Acquity APC, Waters, Milford, CT, USA) equipped with a refractive index (RI) detector (RI Detector, Waters), a multi-angle light scattering (MALS) detector (microDAWN, Wyatt Technology, Santa Barbara, CA, USA), and columns (XT45 (150 mm), XT200 (75 mm), and XT900 (75 mm); Waters) at 40 °C using THF as the mobile phase at a flow rate of 0.6 mL/min (GPC-MALS).

The branch structure of PLA and intrinsic viscosity of PLA solutions were analyzed using a GPC system (Alliance e2695, Waters) equipped with an RI detector (2414, Waters), MALS detector (DAWN 8, Wyatt Technology), viscometer (Visco Star, Wyatt Technology Co.), and columns (LB-803, LB-806 M (× 2), Shoko Science Co., Ltd., Kanagawa, Japan) at 40 °C. DMF containing 10 mmol/L LiBr was used as the mobile phase at a flow rate of 1.0 mL/min (GPC-MALS-VISCO).

2.5. Membrane preparation

Procedure of membrane preparation via NIPS is shown in Scheme 1. For membrane preparation via NIPS, the synthesized PLA samples were dissolved in NMP (good solvent) at 60 °C to prepare 20 wt% PLA solutions [12], which were then aged at 60 °C for 1 h. The solutions were cast onto glass plates (50 °C) using an applicator with a 200-μm gap [16]. The concentration of PLA solution was determined based on reports and our preliminary experimental screening (Fig. S1, Table S1). The glass plates were left to stand for 10 s and then immersed in distilled water (non-solvent) at 25 °C. After 30 min, the glass plates were transferred to fresh distilled water and immersed for more than 15 h. Membranes are denoted by appending "-M" to the PLA sample names (e.g., membranes prepared from L-PLA-100k, 4S-PLA-100k, and 8S-PLA-100k are denoted as L-PLA-100k-M, 4S-PLA-100k-M, and 8S-PLA-100k-M, respectively).

The viscosities of the PLA solutions were measured using plate-cone viscometer (RE-100, Toki Sangyo, Tokyo, Japan). The viscosities were measured at 25 °C in constant temperature room, with the lowest plate rotation speed of the viscometer (0.5 rpm) to minimize the effect of shear on solution viscosity.

2.6. Membrane characterization

2.6.1. FE-SEM observation

For surface observation, membranes were dried under vacuum and coated with osmium prior to analysis. Field-emission scanning electron microscopy (FE-SEM; JSM-7800F, JEOL Ltd.) was performed at an accelerating voltage of 1 kV. For cross-sectional observation, wet membranes were fractured in liquid nitrogen and then dried under vacuum. In this case, the samples were coated with platinum prior to analysis and FE-SEM (JSM-6610LA, JEOL Ltd.) was conducted at an accelerating voltage of 5 kV.

2.6.2. Bulk porosity

The bulk porosity (φ; %) of the membranes was calculated from the weights of the wet membrane (W_{wet}) and corresponding dry membrane (W_{dry}) using Eq. (1):

$$\varphi = \frac{\left(\frac{W_{wet} - W_{dry}}{\rho_{water}}\right)}{\left(\frac{W_{wet} - W_{dry}}{\rho_{water}} + \frac{W_{dry}}{\rho_{PLA}}\right)} \times 100 \quad (1)$$

where ρ_{water} is the density of water (1) and ρ_{PLA} is the density of PLA (1.25) [29].

2.6.3. Water permeance

Pure water permeance was measured by pressurizing distilled water on the top surface (in this study, top surface (the surface facing water during phase separation) had fine pores and bottom surface (the surface facing the glass substrate during phase separation) had macropores (see Scheme 1)). The transmembrane pressure was adjusted to 0.05–0.10 MPa by controlling the valve on the concentrated side. To ensure stable measurements, pure water permeance was measured 40 min after the beginning of pressurization.

2.6.4. Rejection and molecular weight cut-off (MWCO)

The separation performance can be evaluated by determining the

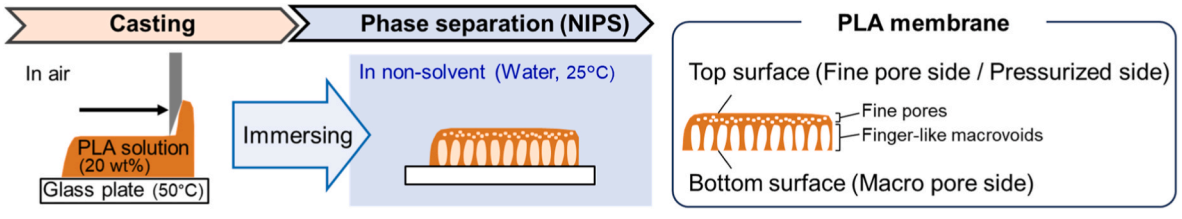

Scheme 1. Procedure of membrane preparation via NIPS and schematic diagram of PLA membrane.

MWCO using PEGs with different molecular weights [30]. PEG 600, PEG 6,000, PEG 10,000, PEG 20,000, PEG 35,000, and PEG 100,000 (each 500 ppm) were dissolved in distilled water to obtain PEG aqueous feed solutions. The solutions were supplied to the membrane at 50–100 kPa under cross-flow filtration with stirring at 800 rpm. The rejection R_i (%) of PEG of molecular weight i was calculated using Eq. (2):

$$R_i = 1 - \left(\frac{C_{pi}}{C_{fi}} \times 100\right) \quad (2)$$

where C_{pi} and C_{fi} are the concentrations of PEG of molecular weight i in the permeate and feed solutions, respectively, determined by GPC with RI detection (GPC-RI) [30]. R_i was determined for PEG with a molecular weight range of 6000–200,000. MWCO was defined as the molecular weight at which R_i reached 90 %. GPC measurements were performed at 40 °C using a GPC system (Nexera, Shimadzu, Kyoto, Japan) equipped with an RI detector (RID-20A, Shimadzu) and two columns (OHpak SB-806 M HQ columns, Shoko Science Co., Ltd.) with an mobile phase flow rate of 1.0 mL/min. The mobile phase was distilled water containing $NaNO_3$ (50 mmol/L) and NaN_3 (0.02 wt%). A calibration curve was prepared using Easi Vial PEG/PEO standards.

2.6.5. Thermal analysis

Differential scanning calorimetry (DSC) thermograms were measured using a DSC module (DSC6200, Hitachi High-Tech Co., Tokyo, Japan) under a nitrogen atmosphere (nitrogen flow rate of 40 mL/min) with a heating/cooling rate of 10 °C/min. Samples were subjected to a heating–cooling–heating cycle between 0 and 190 °C.

2.6.6. Hydrolysis test

Borate buffer (pH 9, 3 mL) was placed in screw-cap vials with a diameter of about 15 mm. Dried PLA membranes (10 × 10 mm) were immersed in the borate buffer. The samples were incubated at 65 °C for 20, 45, 88, 125, and 215 h for alkaline hydrolysis. Hydrolysis condition described above was set as an accelerated aging. The hydrolysis temperature was set at 65 °C, which is above T_g of PLA and thus promotes hydrolysis. At high pH values such as pH 14, hydrolysis occurs too rapidly (80 % of weight was lost in 3 h) and is unsuitable for analysis, therefore, pH 9 was selected. After hydrolysis, the membranes were collected by suction filtration using 1.0-μm membrane filters and then washed with water. The membranes were dried under vacuum for 5 h and then M_n was determined by GPC-MALS (see Section 2.4). The normalized M_n was calculated from the number-average molecular weight after hydrolysis ($M_{n\ after}$) and number-average molecular weight before hydrolysis ($M_{n\ before}$).

$$\text{Normalized } M_n = \frac{M_{n\ after}}{M_{n\ before}} \times 100 \quad (3)$$

3. Results and discussion

3.1. Synthesis of PLA and evaluation of branch structure

To investigate the effects of PLA molecular structure on membrane structure, performance, and hydrolysis behavior, PLAs with comparable M_w but different branch number were synthesized. The star-branched PLA used in this study consisted of PLA arm chains extending from a central initiator, and the target molecular weight of PLA was determined as follows. The entanglement molecular weight (M_e) of PLA is approximately 9000 [31]. Consequently, for star-branched PLA, if the molecular weight of one arm is below M_e, chain entanglement does not occur, resulting in a considerable decrease of mechanical strength. Therefore, M_n must be set so that one chain exceeds M_e. Specifically, for eight-arm star-branched PLA, M_n needed to exceed 72,000 (9000 × eight arms) to ensure entanglement. For this reason, the lower limit of M_n was set as 72,000. When eight-arm star-branched PLA with M_n = 42,000 (M_n of one arm was 5250) was used for membrane preparation, the resulting porous membrane had extremely low mechanical strength and collapsed upon handling. Similarly, for four-arm star-branched PLA, M_n = 36,000 (9000 × four arms) was set as the lower limit of M_n. In addition, because M_w correlates more strongly with physical properties than M_n, synthesis conditions were adjusted to produce PLAs with comparable M_w. In this study, because dispersity was controlled within a narrow range ($M_w/M_n \leq 1.2$), when the lower limit of M_n was 72,000, the corresponding M_w was 86,400 (72,000 × 1.2). We decided to use PLA with a M_w of around 100,000 for membranes.

Polymerization results are summarized in Table 1. A series of linear and branched PLAs (Run 1, 2, and 4–7) were synthesized via ring-opening polymerization of lactide with organocatalyst (Fig. 1(a)). Because linear PLA with M_w = 100,000 was not obtained by this method, we attempted esterification of linear PLA with hydroxyl end groups and another linear PLA with a carboxylic acid terminal group to obtain the desired linear PLA with high M_w [32]. Specifically, linear PLA with hydroxyl groups at both ends (HO-PLA-OH, Run 1) was synthesized and then condensed with linear PLA with a carboxylic acid group at one end and a hydroxyl group at the other end (HOOC-PLA-OH, Run 2) according to Fig. 1(b) to increase M_w. Because the end functional groups are considered to affect the membrane structure and hydrolysis behavior, hydroxyl groups were used as end groups for all PLAs. Fractional precipitation was performed by dissolving the obtained crude PLA in THF and gradually adding methanol to precipitate the desired linear PLA with M_w = 97,000 and M_w/M_n = 1.20 (L-PLA-100k, Table 1, Run 3). Subsequently, four-arm star-branched PLA (4S-PLA-100k, Run 4) and eight-arm star-branched PLA (8S-PLA-100k, Run 5) with M_w comparable to that of L-PLA-100k (Run 3) were synthesized. 4S-PLA-100k and 8S-PLA-100k had M_w of 95,800 and 94,500, respectively, and narrow dispersity ($M_w/M_n \leq 1.20$). ^{1}H NMR spectroscopy measurements revealed that the catalyst was completely removed during purification (Fig. S2(a)–(c)). To evaluate the effect of M_w on membrane structure, performance, and hydrolysis behavior, four-arm star-branched PLAs with different M_w (4S-PLA-65k and 4S-PLA-50k, Run 6 and 7) were synthesized by changing the monomer/initiator ratio and polymerization time of ring-opening polymerization. 4S-PLA-65k and 4S-PLA-50k possessed M_w of 65,900 and 50,000, respectively, and had narrow dispersity ($M_w/M_n \leq 1.20$).

The branch structures of L-PLA-100k, 4S-PLA-100k, and 8S-PLA-100k were analyzed by GPC. A plot of the hydrodynamic radius of PLA molecules in solution against molecular weight M (Fig. 2(a)) indicated that the hydrodynamic radius decreased in the order of L-PLA-100k > 4S-PLA-100k > 8S-PLA-100k. This means that the branching degree of PLA can be controlled by the functional group number of the initiator. This trend was also confirmed from the branching ratio g'_M, which was calculated from the intrinsic viscosities of the branched and linear polymers ($[\eta]_{br}$ and $[\eta]_{lin}$, respectively) using Eq. (4) (Fig. 2(b)) [33]. A smaller g'_M value indicates a higher branch number. Fig. 2(b) shows that the branch number increased in the order of L-PLA-100k < 4S-PLA-100k < 8S-PLA-100k. These results demonstrate that the branch structure of PLA can be effectively controlled by varying the functional group number of the initiator.

$$g'_M = \left(\frac{[\eta]_{br}}{[\eta]_{lin}}\right)_M \quad (4)$$

3.2. Effect of PLA molecular structure on membrane structure

In this section, we examine how PLA molecular structure and molecular weight affect membrane structure. Regarding the membrane preparation conditions, the PLA solution concentration of 20 wt% was determined based on our preliminary experimental screening (Fig. S1 and Table S1). At a lower concentration (10 wt%), the resulting membranes exhibited insufficient mechanical strength. In contrast, at a higher concentration (30 wt%), although the mechanical strength was improved, surface pores were hardly observable by SEM, making the

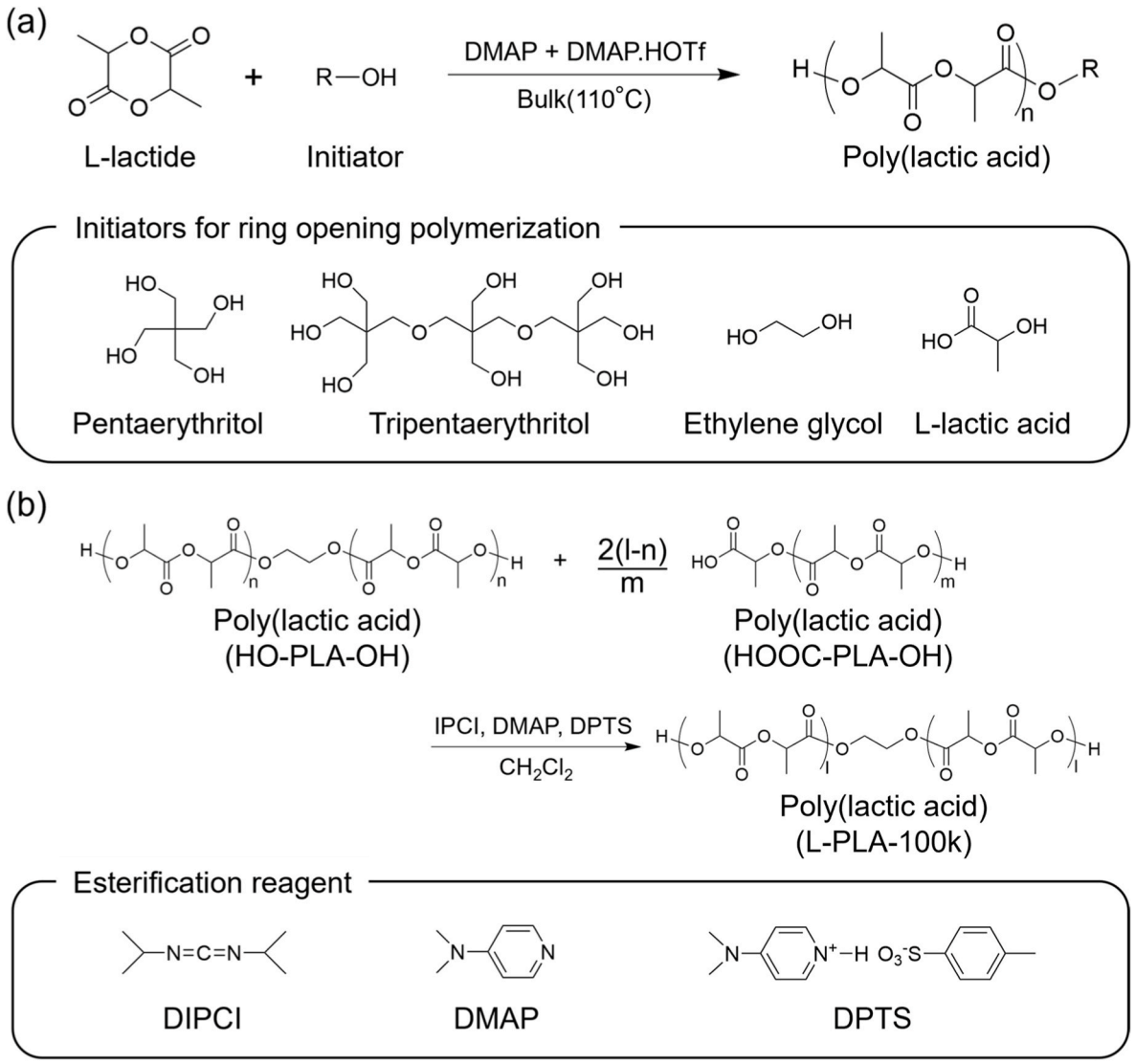

Fig. 1. Synthesis of PLA. (a) Ring-opening polymerization of L-lactide with organocatalyst. (b) Esterification of HO-PLA-OH and HOOC-PLA-OH to synthesize L-PLA-100k.

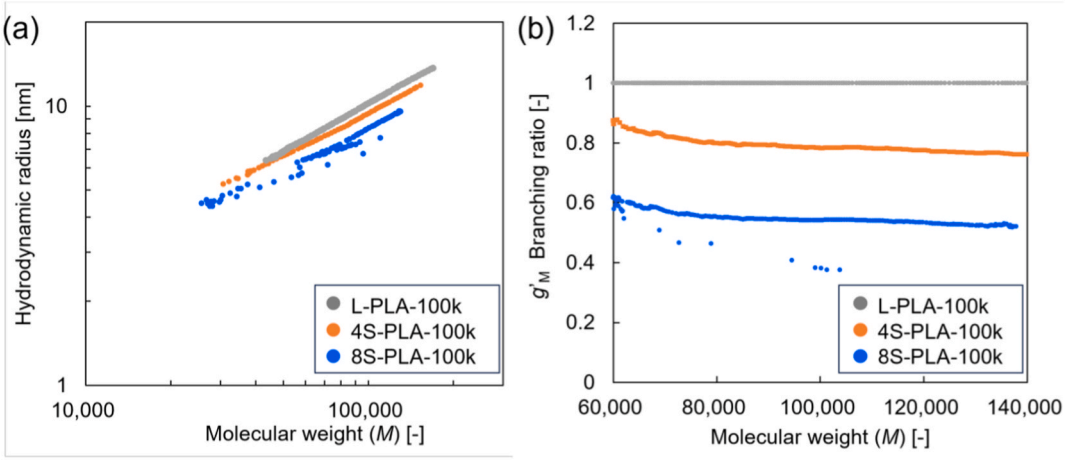

Fig. 2. (a) Relationship between the molecular weight and hydrodynamic radius of PLA. (b) Relationship between the molecular weight and branching ratio of PLA. Horizontal axes represent the molecular weight distribution obtained by GPC, not average molecular weight.

membranes unsuitable for structural characterization. Therefore, 20 wt % was selected as a balanced condition that allows the formation of

mechanically stable membranes with clearly observable surface pores, enabling both performance evaluation and structural analysis.

Membranes were prepared using PLAs with similar M_w (~100,000) but different branch number and then their structures were observed by FE-SEM (Fig. 3(a)–(c), Fig. S3(a)–(c)). The finest pores were formed on the membrane surface that faced the solvent during phase separation (top surface). 8S-PLA-100k-M (Fig. 3(c2)) exhibited the largest pore diameter of the membranes. Cross-sectional FE-SEM images (Fig. 3(a3), (b3), and (c3)) revealed that all PLA membranes possessed the characteristic finger-like macrovoid structure derived from the NIPS method. In the membranes, the fine pores in the top surface have the strongest effect on separation and permeability performance; therefore, FE-SEM

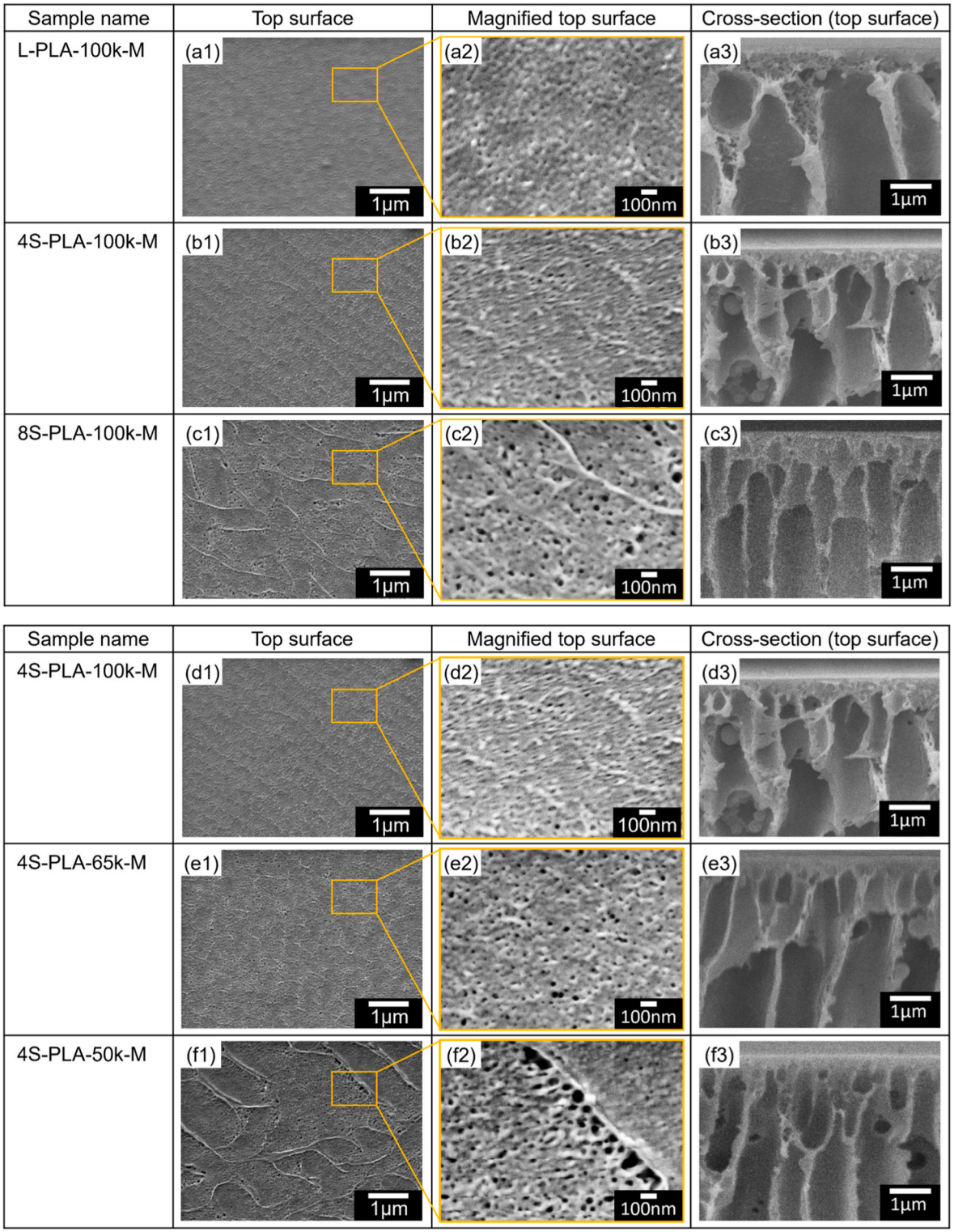

Fig. 3. FE-SEM images of (a)–(c) PLA membranes with similar weight-average molecular weight M_w and different branch number, and (d)–(f) four-arm star-branched PLA membranes with different M_w. (b) and (d) show FE-SEM images of the same membrane. "Top surface" and "bottom surface" indicates the surfaces of non-solvent facing and glass plate facing side during phase separation, respectively (see Scheme 1).

images of the membrane top surfaces (Fig. 3(a2), (b2), (c2)) were analyzed. The results (Fig. 4(a) and Table 2) indicated that membranes with a higher branch number exhibit larger pore diameter in their top surface. In particular, the pore size distribution of 8S-PLA-100k-M with the largest branch number of the membranes showed an increase in the number of large pores with diameters exceeding 50 nm (Fig. 4(a)).

Next, to investigate the effect of M_w on membrane structure, membranes were prepared from four-arm star-branched PLAs with different M_w. The structures of these membranes were observed by FE-SEM (Fig. 3 (d)–(f), Fig. S3(d)–(f)). The top surface again contained the finest pores, and 4S-PLA-50k-M (Fig. 3(f2)) had the largest pore diameter among the membranes. Cross-sectional FE-SEM images (Fig. 3(d3), (e3), and (f3)) revealed the presence of finger-like macrovoid structures in all membranes. The image analysis results of top surface (the surfaces with fine pores) are presented in Fig. 4(b) and Table 2. Membranes prepared from PLAs with lower M_w tended to have pores with larger diameters in their top surfaces. In particular, 4S-PLA-50k-M, which was the PLA with the lowest M_w, exhibited pores exceeding 100 nm, as shown in Fig. 3(f2) and in its pore size distribution in Fig. 4(b).

3.3. Effect of PLA molecular structure on membrane performance

Subsequently, we investigated how molecular structure and M_w affect membrane performance. The separation performance of membranes prepared from PLAs with similar M_w (~100,000) but different branch numbers was evaluated (Fig. 5(a), Table 2). Membranes with higher branch number exhibited larger MWCO values determined with PEG, indicating larger pore diameters than those of membranes with lower branch number. Next, the separation performance of membranes prepared from four-arm star-branched PLAs with different M_w was evaluated (Fig. 5(b)–Table 2). The results indicated that membranes composed of PLAs with lower M_w showed higher MWCO values and larger pore size than those of membranes prepared from PLAs with higher M_w. 4S-PLA-50k-M with the lowest M_w of the membranes rejected <95 % of PEG with high molecular weight (above 100,000), indicating the presence of larger pores. The MWCO results displayed similar trends to those of the FE-SEM analysis (Fig. 4, Table 2), confirming that the pore structure of the membrane top surface strongly influences separation performance.

The permeance of the PLA membranes (Table 2) differed by up to 20 times (4S-PLA-100k-M and 8S-PLA-100k-M). Therefore, we investigated the parameters of membrane structure that affect permeance. Note that diameter equivalent to MWCO [nm] was calculated by assigning MWCO to the PEG molecular weight (M) using Eq. (5) [34] which used for determining the PEG molecular diameter (D [nm]):

$$D\,[nm] = 33.46 \times 10^{-3} \times M^{0.557} \quad (5)$$

It should be noted that this pore diameter represents an apparent or effective value derived from MWCO, rather than a directly measured pore size. Parameters affecting permeance may include pore diameter, surface porosity, and bulk porosity as well as internal structural features such as tortuosity and effective flow-path length. The bulk porosity determined from water content was about 80 % for all membranes (Table 2), indicating that differences in permeance were not caused by bulk porosity. A clear relationship between permeance and the square of pore diameter (Fig. S4(a)) was observed. Furthermore, a strong relationship was observed with top-surface porosity (Fig. S4(b)), suggesting that surface porosity is the dominant factor affecting permeance. A strong relationship between permeance and the product of the square of pore diameter and surface porosity (equivalent to the fourth power of pore diameter) was observed (Fig. 6(a)). This correlation is qualitatively consistent with a Hagen–Poiseuille-type dependence and can serve as an engineering-level description of the observed permeance trends. However, given that part of the pore diameter is derived from MWCO and NIPS membranes typically exhibit asymmetric structures such as finger-like macrovoids and a dense skin layer, this relationship should not be interpreted as a deterministic transport mechanism. Instead, it should be regarded as an approximate or empirical correlation under the current dataset and structural assumptions.

We next considered the factors causing differences in membrane structure based on molecular structure and molecular weight. Although crystallization can influence phase separation in some cases [35], no melting peaks (typically observed at 160–180 °C) were detected in the DSC thermograms of any PLA membranes (Fig. 6(b)). This result

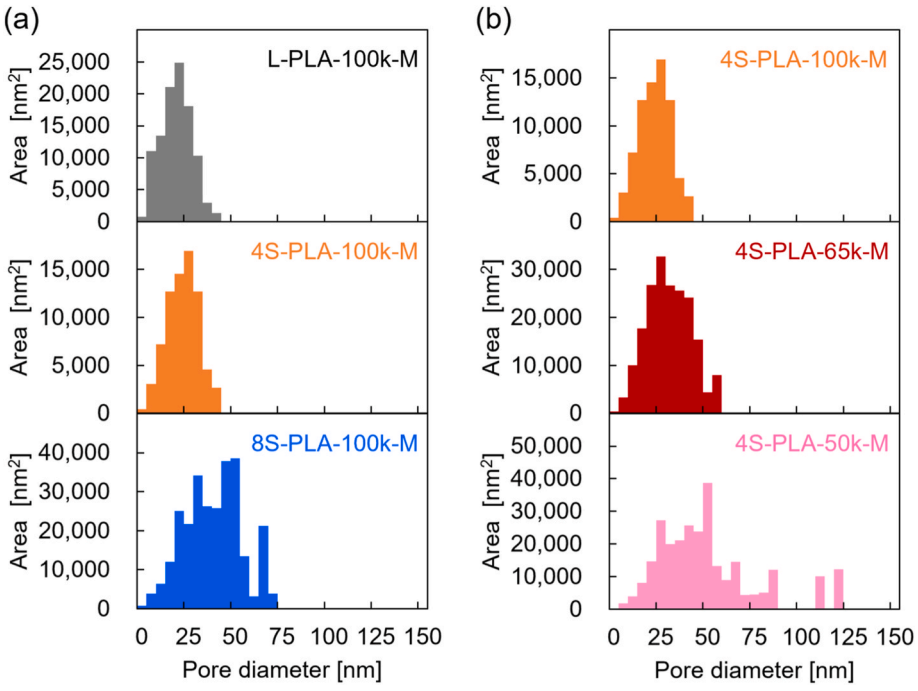

Fig. 4. Pore diameter distribution (top surface) of PLA membranes obtained by FE-SEM image analysis. (a) PLA membranes with similar weight-average molecular weight M_w and different branch number. (b) Four-arm star-branched PLA membranes with different M_w.

Table 2
Structure, permeability, and separation performance of PLA membranes.

Sample	Pore diameter [a] (top surface)		Aperture ratio [a] (top surface)	Porosity [b] (bulk)	Water permeance	MWCO	Diameter equivalent to MWCO
	Average	C. V. [c]					
	[nm]	[%]	[%]	[%]	[L/(m^2 h bar)]	[−]	[nm]
L-PLA-100k-M	12	61	6.2	80.1	13	15,000	7.1
4S-PLA-100k-M	14	65	4.5	79.8	8.0	17,000	7.6
8S-PLA-100k-M	22	72	18	80.3	160	52,000	14
4S-PLA-65k-M	20	58	12	80.0	90	47,000	13
4S-PLA-50k-M	27	69	16	79.7	140	52,000	14

[a] Calculated by FE-SEM image analysis.
[b] Measured by water content.
[c] Coefficient of value = (standard deviation/average) × 100.

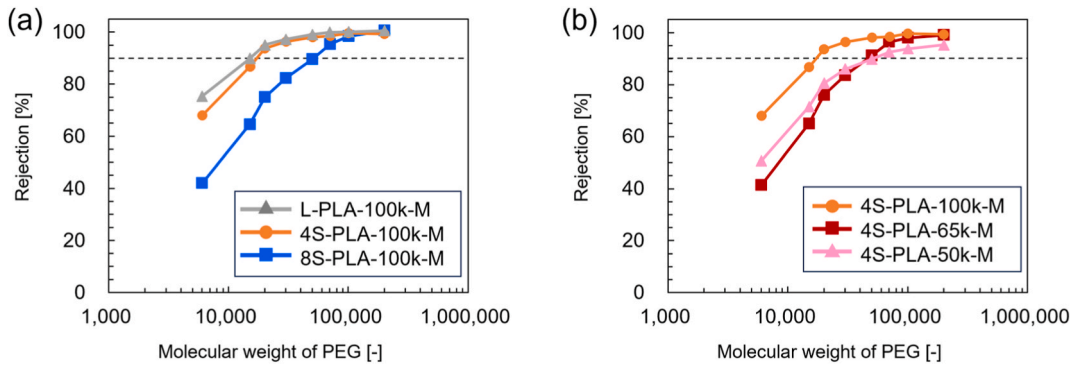

Fig. 5. MWCO of PLA membranes determined with PEG. (a) PLA membranes with similar M_w and different branch number. (b) Four-arm star-branched PLA membranes with different M_w. Horizontal axes represent the molecular-weight distribution obtained by GPC, not average molecular weight.

indicates that all samples were amorphous and crystallization did not contribute to the observed structural changes. The small endothermic peak around 60 °C is attributed to enthalpy relaxation rather than melting (DSC thermograms of PLA membranes in the first cooling and second heating steps are shown in Fig. S5(a) and (b).) Next, we focused on the viscosity of PLA solution in phase separation. For the same M_w, an increase in the branch number of star-branched polymers lowers molecular entanglement, leading to a decrease in intrinsic viscosity [η] [36]. In the case of the same branch number, a decrease of M_w leads to a decrease of [η] according to the Mark–Houwink–Sakurada equation:

$$[\eta] = K \cdot M_w^a \quad (6)$$

where K and a are constants determined by polymer structure, solvent, and temperature. Therefore, we focused on the solution viscosity as a factor that might affect the membrane structure. Although the results were obtained using DMF/LiBr as the mobile phase, GPC-MALS-VISCO measurements showed that [η] decreases with increasing PLA branch number or decreasing M_w (Fig. 6(c)). Both M_w and [η] changes followed the Mark–Houwink–Sakurada equation (Eq. (6)). Since PLA solutions with a concentration of 20 wt% (solvent: NMP) was used in membrane preparation, the viscosity (η) of this solution was measured using a viscometer (Fig. 6(d)). Although Fig. 6(c) and (d) correspond to different PLA concentrations and represent the dilute and concentrated solution regimes, respectively, no significant differences were observed in the relationships between M_w, branch number and viscosity in these two regimes.

It is considered that lower viscosity promotes faster molecular movement in the PLA solution and faster structure growth during phase separation [37,38], which leads to larger pore diameter and higher surface porosity. Fig. 6(e) indicates that membranes prepared from solutions with lower η values tend to have larger MWCO (i.e., larger pore diameter). A previous study on separation membranes using stereocomplex PLA indicated that increasing the stereocomplex ratio lowered the viscosity of the preparation solution [16]. Furthermore, membranes with larger pore diameter and higher water flux were obtained at lower viscosities [16], consistent with this study. Simulations exploring the relationship between phase separation structure and polymer relaxation time showed that shorter relaxation times lead to faster structural development and the formation of larger phase separation structures [37]. Relaxation time shortens as the viscosity of a polymer solution decreases [37]. As shown in Fig. 6(d), both an increase of branch number and decrease of M_w resulted in lower η, indicating that the relaxation time was also shortened. Therefore, it is considered that the shorter relaxation time caused by a higher branch number or lower M_w promoted development of phase separation structure, leading to the formation of larger pores and increased surface porosity. Overall, the observed changes in membrane structure with increasing branch number or decreasing M_w can be attributed to decreased chain entanglement, which led to lower viscosity and shorter relaxation times during phase separation.

The tensile test results (Table S2) showed that decreasing of the branch number or increasing of the M_w tended to result in higher tensile strength and higher elongation at break. In addition to this, 8S-PLA-100k-M exhibited higher permeation performance compared with 4S-PLA-50k-M (with a comparable MWCO), while the strength and elongation of 8S-PLA-100k-M were slightly higher than 4S-PLA-50k-M. Therefore, when aiming to achieve large pore size and high permeation performance, increasing the branch number is considered to be more advantageous than reducing the molecular weight.

In this study, it is necessary to distinguish the effects of branch number and M_w of PLA on membrane properties into direct and indirect contributions. For example, branch number and M_w directly change microscopic factors of molecular structure such as branching point density and chain packing density, thereby affecting chain entanglement and exerting a direct influence on the mechanical strength of the

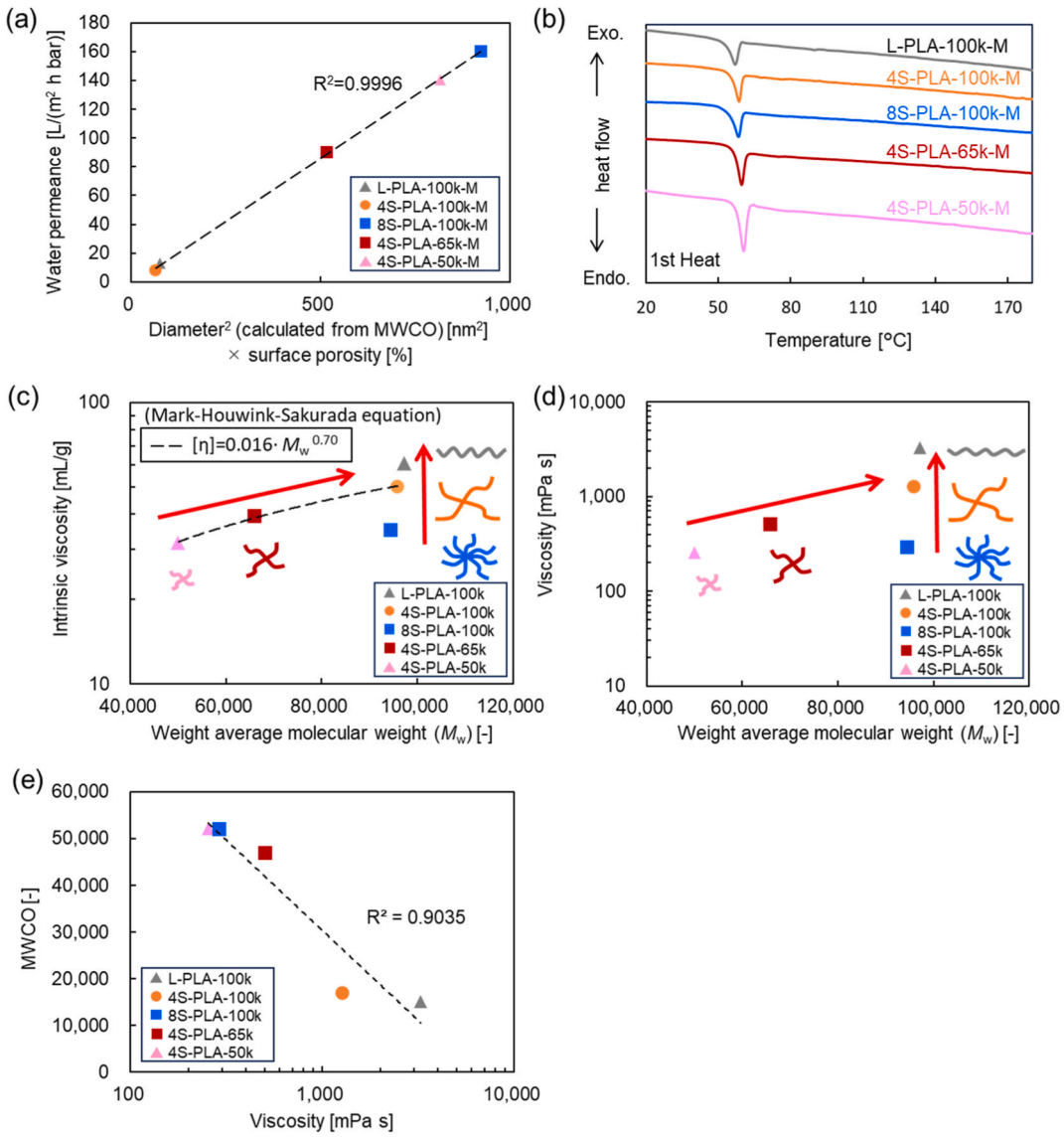

Fig. 6. (a) Relationship between pore diameter, surface porosity, and water permeance of PLA membranes. (b) DSC thermograms of PLA membranes (first heating run). The curves are shifted vertically for clarity. (c) Relationship between intrinsic viscosity ([η]) measured by GPC-MALS-VISCO using DMF/LiBr solution, weight-average molecular weight (M_w), and branch number for each PLA. (d) Relationship between viscosity (η) of 20 wt% PLA solution (solvent: NMP) measured by viscometer, M_w, and branch number for each PLA. (e) Relationship between MWCO of PLA membranes and η of 20 wt% PLA solution (solvent: NMP).

membranes. On the other hand, the branch number and M_w also change solution viscosity and consequently affect phase separation behavior, which induces variations in the macroscopic factors: porous membrane structure. As a result, they are considered to indirectly influence mechanical strength through changes in membrane structure. Similarly, the branch number and M_w are considered to indirectly affect membrane structure and the associated membrane performance. Thus, it should be noted that the branch number and M_w of PLA exert combined effects on the membrane properties. Regarding membrane structural design, it was clarified that the use of linear PLA leads to membranes with finer pore sizes and higher mechanical strength, whereas the use of eight-arm star-branched PLA results in membranes with larger pore sizes and higher water permeance.

Table 3 provides a comparative summary of the performance of our PLA membranes with previously reported membranes. Although direct comparison is qualitative only because previous studies used bovine serum albumin (BSA) (molecular weight = 66,000) for rejection tests, the permeance of our membranes lies between those of membranes reported by Moriya et al. [12] and Shen et al. [39]. The rejection performance of our membranes is higher than that of many reported membranes. Improvement of membrane preparation by controlling branch shape (e.g., comb-like or long-chain branching) and solution viscosity during phase separation in addition to branch number and

Table 3
Comparison of the performance of current and previously reported PLA membranes.

Membrane	Water permeance [L/(m² h bar)]	Rejection [%]	Reference
PLA (8S-PLA-100k-M)	160	PEG: 94	This study
PLA (stereocomplex)	3325	BSA: 90	Zhu Xiong et al. [16]
PLA	880	BSA: 80	Moriya et al. [12]
PLA + PLA-co-PEG (3 wt %)	110	BSA: ~100	Shen et al. [39]
PLA + PBS(2 wt%) blend	18	BSA: 88	Keawsupsak et al. [40]

BSA: molecular weight = 66,000, PEG: molecular weight = 66,000.

molecular weight is expected to further enhance both membrane permeance and separation performance.

3.4. Effect of molecular structure on the hydrolysis of PLA membranes

Finally, we investigated how molecular structure and M_w affect the hydrolysis behavior of PLA membranes. As a normal hydrolysis test, PLA membranes were immersed in phosphate buffer (pH 7) at 35 °C, and no change of M_n was observed. Then, as an accelerated hydrolysis test, membranes with different branch number were immersed in borate buffer (pH 9) at 65 °C and the change of M_n was monitored to investigate the effect of branch structure on hydrolysis. Because hydrolysis involves chemical reactions, M_n changes were analyzed according to a previous study [23]. Fig. 7(a) shows the time-dependent change of normalized M_n during hydrolysis (Not normalized M_n were shown in Fig. S6). Up to ~88 h, the order of normalized M_n from highest to lowest was L-PLA-100k-M > 8S-PLA-100k-M > 4S-PLA-100k-M; thereafter, the order changed to 8S-PLA-100k-M > L-PLA-100k-M > 4S4-PLA-100k-M. It is considered that the molecular chain density in star-branched polymers is higher near branch points (derived from the initiator) and decreases toward chain ends. Because the density near branch points increases with branch number, it is considered that water penetration and hydrolysis are inhibited more strongly near the branch points with increasing branch number. Therefore, the four- and eight-arm star--branched PLAs, which have a larger proportion of chain-end segments with lower density than that of linear PLA, are hydrolyzed faster than linear PLA initially. However, as hydrolysis proceeds, the eight-arm star-branched PLA, which is the most resistant to hydrolysis around the branch point, may begin to decompose more slowly than the other samples. To experimentally investigate the relationship between branch number and water penetration described above, Fourier transform infrared spectroscopy (FTIR) was employed to evaluate water uptake (Fig. S7 and Table S3). To eliminate the influence of porous structures, nonporous PLA films (see supplementary information section 1.2.) were used, and they were immersed in borate buffer (pH 9) at 65 °C for 88h before FTIR measurement. Since the O–H stretching vibration originating from absorbed water appears at 3654 cm^{-1} [41,42], the water uptake of each PLA sample was compared using the ratio of the O–H peak intensity to that of the methine groups of the PLA backbone (2882 cm^{-1}). As shown in Fig. S7 and Table S3, the water uptake decreases with increasing branch number, suggesting that a higher density of branching points suppresses water penetration into the polymer matrix. Therefore, PLA with higher branch number may suppress water penetration, and thus, hydrolysis proceeds more slowly. Meanwhile, chain-end segments with lower density in branched PLA may promote hydrolysis as described above. Therefore, the balance between densities of branching point and chain-end segments is important to promote hydrolysis. These findings suggest that at M_w ~100,000, four-arm star-branched PLA has a suitable balance of these to promote hydrolysis.

Next, to evaluate the effect of M_w on hydrolysis behavior, the hydrolysis of membranes composed of four-arm star-branched PLAs of different M_w was evaluated. Fig. 7(b) shows the time-dependent change of normalized M_n of the membranes. Across the hydrolysis period, membranes with higher initial molecular weight were hydrolyzed more rapidly. This may be attributed to the fact that for PLA with lower M_w, the ratio of branch points (derived from the initiator) to molecular weight is higher, resulting in higher local chain density near the branch points, which inhibits water penetration and hydrolysis. As shown in Fig. S7 and Table S3, the water uptake decreases with increasing M_w, indicating that an increased density of branching points suppresses water penetration into the polymer matrix. They also support that the balance between densities of branching point and chain-end segments is important to promote hydrolysis as described above. Therefore, for four-arm star-branched PLA, increasing M_w appears to promote hydrolysis.

Crystalline domains hydrolyze more slowly than amorphous ones in biodegradable polymers [43]. DSC measurements (Fig. 6(b)) revealed no obvious melting peaks in the thermograms of the membranes, confirming their amorphous state. Therefore, the difference in the hydrolysis behavior of the membranes cannot be attributed to the presence of crystalline domains.

In the same manner as discussed in Section 3.3, the effects of branch number and M_w on hydrolysis behavior were also classified into direct and indirect contributions. Branch number and M_w directly change factors of molecular structure such as branching point density and chain packing density, thereby directly influencing hydrolysis behavior. In addition, they also affect for membrane porous structure inducing change of surface area, which alters water uptake behavior as an indirect effect. However, since the hydrolysis tests in this study were conducted above T_g of PLA, thermal shrinkage occurred at a very early stage (within 20 h), making it difficult to systematically evaluate the influence of membrane structure on hydrolysis behavior in the present work. From the viewpoint of molecular design for hydrolysis properties, a moderate branch number, such as that of four-arm PLA, is effective in accelerating hydrolysis, whereas linear and highly branched structures (eight-arm PLA) require longer hydrolysis times. As described above, it should be noted that the branch number and M_w of PLA exert combined effects on the membrane structure, membrane properties, and hydrolysis behaviors.

For practical application of PLA membranes in water treatment, antifouling performance and long-term operational stability are important. Since PLA is hydrophobic polymer [44], blending or surface modification with hydrophilic polymers can enhance surface hydrophilicity and potentially improve antifouling performance. In addition, long-term operational test is necessary to investigate stability of

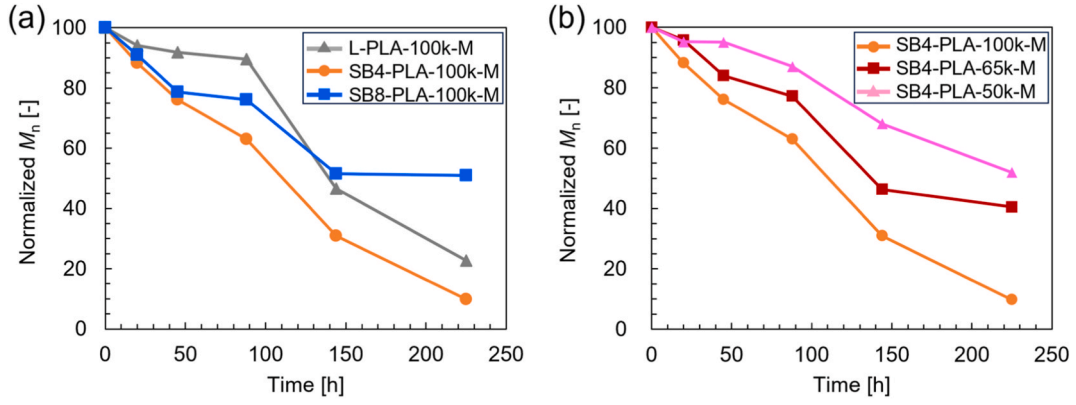

Fig. 7. Time-dependent change of normalized number-average molecular weight M_n during hydrolysis tests. (a) PLA membranes with similar M_w and different branch number. (b) Four-arm star-branched PLA membranes with different M_w.

blending, surface modification and membrane performance. In an economic perspective, commercial PLA resins are available at costs comparable to or lower than those of conventional membrane polymers such as polysulfone and polyvinylidene fluoride, and PLA membranes can be prepared via NIPS process, suggesting potential for cost-competitive commercialization.

4. Conclusion

PLAs with varied molecular structures were synthesized via ring-opening polymerization with an organocatalyst. GPC measurements confirmed narrow molecular-weight distributions with controlled branch structure and molecular weight. Porous membranes prepared from the PLAs via NIPS demonstrated that both higher branch number and lower M_w led to increased MWCO. This behavior is attributed to decreased solution viscosity promoting development of phase separation. The membranes exhibited relatively high MWCO compared with that of previously reported PLA membranes. Further improvement of casting conditions is expected to increase permeance and separation performance.

In accelerated hydrolysis tests, the decrease ratio of molecular weight at 215 h was the largest for four-arm star-branched PLA. This suggests that moderate branch number accelerates hydrolysis, whereas excessive branch number inhibits water penetration and hydrolysis around the branch core. For the four-arm star-branched PLA membranes, higher M_w increased the hydrolysis rate, which is possibly caused by the greater fraction of rapidly hydrolyzable arm segments. Overall, this study demonstrates that both the performance and hydrolizability of sustainable PLA UF membranes can be enhanced by controlling PLA branch structure and molecular weight.

CRediT authorship contribution statement

Koichi Takada: Writing – original draft, Project administration, Methodology, Investigation, Funding acquisition, Formal analysis, Conceptualization. **Akinori Okada:** Writing – review & editing, Methodology, Investigation. **Hiroshi Hirano:** Writing – review & editing, Methodology. **Joji Kadota:** Writing – review & editing, Methodology, Investigation, Funding acquisition. **Tooru Kitagawa:** Writing – review & editing, Methodology, Investigation. **Hideto Matsuyama:** Writing – review & editing, Supervision. **Tomohisa Yoshioka:** Writing – review & editing, Supervision, Funding acquisition. **Keizo Nakagawa:** Writing – review & editing, Supervision, Project administration, Methodology, Investigation, Funding acquisition.

Funding

This work was supported by the Japan Society for the Promotion of Science (JSPS) KAKENHI Grant Number JP25K08373.

Declaration of competing interest

The authors declare the following financial interests/personal relationships which may be considered as potential competing interests:

Hideto Matsuyama is an Editor of the journal but was not involved in the paper review or handling of this paper.

Appendix A. Supplementary data

Supplementary data to this article can be found online at https://doi.org/10.1016/j.memsci.2026.125225.

Data availability

Data will be made available on request.

References

[1] A. Basko, K. Pochivalov, Current state-of-the-art in membrane formation from ultra-high molecular weight polyethylene, Membranes 12 (2022) 1137, https://doi.org/10.3390/membranes12111137.
[2] A. Hanen, K. Fatma, A. Hiba, H. Khaoula, C. Béchir, A. Qusay, Novel composite membrane based on recycled low-density polyethylene-alumina used for vacuum membrane distillation, Bull. Natl. Res. Cent. 47 (2023) 4–11, https://doi.org/10.1186/s42269-023-01103-z.
[3] C. Hackett, D. Hale, B. Bair, G.D. Manson-Endeboh, X. Hao, X. Qian, S. Ranil Wickramasinghe, A. Thompson, Polysulfone ultrafiltration membranes fabricated from green solvents: significance of coagulation bath composition, Sep. Purif. Technol. 332 (2024) 125752, https://doi.org/10.1016/j.seppur.2023.125752.
[4] S. Gunes-Durak, Development of microfiltration membranes based on polysulfone and polyetherimide blends, Water Sci. Technol. 89 (2024) 2558–2576, https://doi.org/10.2166/wst.2024.135.
[5] S. Ashtiani, M. Khoshnamvand, P. Čífal, M. Dendisová, A. Randová, D. Bouša, A. Shaliutina-Kolešová, Z. Sofer, K. Friess, Fabrication of a PVDF membrane with tailored morphology and properties: via exploring and computing its ternary phase diagram for wastewater treatment and gas separation applications, RSC Adv. 10 (2020) 40373–40383, https://doi.org/10.1039/d0ra07592b.
[6] A. Ghobadi Moghadam, A. Hemmati, Improved water purification by PVDF ultrafiltration membrane modified with GO-PVA-NaAlg hydrogel, Sci. Rep. 13 (2023) 1–16, https://doi.org/10.1038/s41598-023-35027-5.
[7] F. Galiano, K. Briceño, T. Marino, A. Molino, K.V. Christensen, A. Figoli, Advances in biopolymer-based membrane preparation and applications, J. Membr. Sci. 564 (2018) 562–586, https://doi.org/10.1016/j.memsci.2018.07.059.
[8] J. Yu, S. Xu, B. Liu, H. Wang, F. Qiao, X. Ren, Q. Wei, PLA bioplastic production: from monomer to the polymer, Eur. Polym. J. 193 (2023) 112076, https://doi.org/10.1016/j.eurpolymj.2023.112076.
[9] T. Tanaka, D.R. Lloyd, Formation of poly(L-lactic acid) microfiltration membranes via thermally induced phase separation, J. Membr. Sci. 238 (2004) 65–73, https://doi.org/10.1016/j.memsci.2004.03.020.
[10] T. Tanaka, M. Ueno, Y. Watanabe, T. Kouya, M. Taniguchi, D.R. Lloyd, Poly(L-lactic acid) microfiltration membrane formation via thermally induced phase separation with drying, J. Chem. Eng. Japan 44 (2011) 467–475, https://doi.org/10.1252/jcej.11we030.
[11] T. Tanaka, T. Nishimoto, K. Tsukamoto, M. Yoshida, T. Kouya, M. Taniguchi, D. R. Lloyd, Formation of depth filter microfiltration membranes of poly(l-lactic acid) via phase separation, J. Membr. Sci. 396 (2012) 101–109, https://doi.org/10.1016/j.memsci.2012.01.002.
[12] A. Moriya, T. Maruyama, Y. Ohmukai, T. Sotani, H. Matsuyama, Preparation of poly(lactic acid) hollow fiber membranes via phase separation methods, J. Membr. Sci. 342 (2009) 307–312, https://doi.org/10.1016/J.MEMSCI.2009.07.005.
[13] A. Moriya, P. Shen, Y. Ohmukai, T. Maruyama, H. Matsuyama, Reduction of fouling on poly(lactic acid) hollow fiber membranes by blending with poly(lactic acid)-polyethylene glycol-poly(lactic acid) triblock copolymers, J. Membr. Sci. 415–416 (2012) 712–717, https://doi.org/10.1016/j.memsci.2012.05.059.
[14] Q. Xing, X. Dong, R. Li, H. Yang, C.C. Han, D. Wang, Morphology and performance control of PLLA-based porous membranes by phase separation, Polymer (Guildf.) 54 (2013) 5965–5973, https://doi.org/10.1016/j.polymer.2013.08.007.
[15] E. Al Tawil, A. Monnier, Q.T. Nguyen, B. Deschrevel, Microarchitecture of poly (lactic acid) membranes with an interconnected network of macropores and micropores influences cell behavior, Eur. Polym. J. 105 (2018) 370–388, https://doi.org/10.1016/j.eurpolymj.2018.06.012.
[16] Z. Xiong, Y. Zhong, H. Lin, F. Liu, T. Li, J. Li, PDLA/PLLA ultrafiltration membrane with excellent permeability, rejection and fouling resistance via stereocomplexation, J. Membr. Sci. 533 (2017) 103–111, https://doi.org/10.1016/j.memsci.2017.03.028.
[17] Y. Su, Y. Zhao, W. Zheng, H. Yu, Y. Liu, L. Xu, Asymmetric Sc-PLA membrane with multi-scale microstructures: wettability, antifouling, and oil-water separation, ACS Appl. Mater. Interfaces 12 (2020) 55520–55526, https://doi.org/10.1021/acsami.0c17545.
[18] X. Liu, X. Lu, Z. Wang, X. Yang, G. Dai, J. Yin, Y. Huang, Effect of bore fluid composition on poly(lactic-co-glycolic acid) hollow fiber membranes fabricated by dry-jet wet spinning, J. Membr. Sci. 640 (2021) 119784, https://doi.org/10.1016/j.memsci.2021.119784.
[19] T.H. Thi, M. Matsusaki, H. Hirano, H. Kawano, Y. Agari, M. Akashi, Mechanism of high thermal stability of commercial polyesters and polyethers conjugated with bio-based caffeic acid, J. Polym. Sci. Part A Polym. Chem. 49 (2011) 3152–3162, https://doi.org/10.1002/pola.24752.
[20] Z. He, L. Jiang, Y. Chuan, H. Li, M. Yuan, Ring-opening polymerization of L-lactic acid O-carboxyanhydrides initiated by alkoxy rare earth compounds, Molecules 18 (2013) 12768–12776, https://doi.org/10.3390/molecules181012768.
[21] M.C. D'Alterio, I. D'Auria, L. Gaeta, C. Tedesco, S. Brenna, C. Pellecchia, Are well performing catalysts for the ring opening polymerization of l -Lactide under mild laboratory conditions suitable for the industrial process? The case of new highly active Zn(II) catalysts, Macromolecules 55 (2022) 5115–5122, https://doi.org/10.1021/acs.macromol.2c00719.
[22] J. Lunt, Large-scale production, properties and commercial applications of poly lactic acid polymers, Polym. Degrad. Stab. 59 (1998) 145–152, https://doi.org/10.1016/s0141-3910(97)00148-1.
[23] K. Numata, A. Finne-Wistrand, A.C. Albertsson, Y. Doi, H. Abe, Enzymatic degradation of monolayer for poly(lactide) revealed by real-time atomic force microscopy: effects of stereochemical structure, molecular weight, and molecular

branches on hydrolysis rates, Biomacromolecules 9 (2008) 2180–2185, https://doi.org/10.1021/bm800281d.
[24] J.L. Atkinson, S. Vyazovkin, Dynamic mechanical analysis and hydrolytic degradation behavior of linear and branched poly(L-lactide)s and poly(l-lactide-co-glycolide)s, Macromol. Chem. Phys. 214 (2013) 835–843, https://doi.org/10.1002/macp.201200622.
[25] K. Numata, R.K. Srivastava, A. Finne-Wistrand, A.C. Albertsson, Y. Doi, H. Abe, Branched poly(lactide) synthesized by enzymatic polymerization: effects of molecular branches and stereochemistry on enzymatic degradation and alkaline hydrolysis, Biomacromolecules 8 (2007) 3115–3125, https://doi.org/10.1021/bm700537x.
[26] F. Tasaka, Y. Ohya, T. Ouchi, Synthesis of novel comb-type polylactide and its biodegradability, Macromolecules 34 (2001) 5494–5500, https://doi.org/10.1021/ma010067m.
[27] J. Kadota, D. Pavlović, J.P. Desvergne, B. Bibal, F. Peruch, A. Deffieux, Ring-opening polymerization of l-lactide catalyzed by an organocatalytic system combining acidic and basic sites, Macromolecules 43 (2010) 8874–8879, https://doi.org/10.1021/ma101688d.
[28] J. Kadota, D. Pavlović, H. Hirano, A. Okada, Y. Agari, B. Bibal, A. Deffieux, F. Peruch, Controlled bulk polymerization of l-lactide and lactones by dual activation with organo-catalytic systems, RSC Adv. 4 (2014) 14725–14732, https://doi.org/10.1039/c4ra01239a.
[29] G. Dharmalingam, M. Arun Prasad, S. Salunkhe, Investigation of impact strength at different infill rates biodegradable PLA constituent through fused deposition modeling, Mater. Today Proc. 62 (2022) 551–558, https://doi.org/10.1016/j.matpr.2022.03.591.
[30] H. Ohya, A. Haio, Y. Negishi, K. Matsumoto, Standardization method for molecular weight cut-off evaluation of ultrafiltration membranes II. Measurement of molecular weight cut-off using GPC analysis method, Membrane 15 (1990) 62–71, https://doi.org/10.5360/membrane.15.62.
[31] J.R. Dorgan, J.S. Williams, D.N. Lewis, Melt rheology of poly(lactic acid): entanglement and chain architecture effects, J. Rheol. (N. Y. N. Y). 43 (1999) 1141–1155, https://doi.org/10.1122/1.551041.
[32] M. Jikei, C. Terata, K. Matsumoto, Synthesis and properties of long-chain branched poly(L-lactide)s by self-polycondensation of AB2 macromonomers, Mater. Today Commun. 20 (2019) 100528, https://doi.org/10.1016/j.mtcomm.2019.05.004.
[33] B.H. Zimm, R.W. Kilb, Dynamics of branched polymer molecules in dilute solution, J. Polym. Sci. 37 (1959) 19–42, https://doi.org/10.1002/pol.1959.1203713102.
[34] S. Singh, K.C. Khulbe, T. Matsuura, P. Ramamurthy, Membrane characterization by solute transport and atomic force microscopy, J. Membr. Sci. 142 (1998) 111–127, https://doi.org/10.1016/S0376-7388(97)00329-3.
[35] X. Sun, Y. Meng, K. Hu, J. Sun, C. Zhou, C. Su, L. Zhang, C. Zhang, Z. Ma, Crystallization-driven formation of cluster assemblies on surface for super-hydrophobic poly (L-lactic acid)/ZnO composite membrane, Int. J. Biol. Macromol. 283 (2024) 137815, https://doi.org/10.1016/j.ijbiomac.2024.137815.
[36] T. Masuda, Y. Ohta, T. Yamauchi, S. Onogi, Characterization and rheological properties of multi-branched star polystyrenes, Polym. J. 16 (1984) 273–291, https://doi.org/10.1295/polymj.16.273.
[37] H. Tanaka, T. Araki, Viscoelastic phase separation in soft matter: numerical-simulation study on its physical mechanism, Chem. Eng. Sci. 61 (2006) 2108–2141, https://doi.org/10.1016/j.ces.2004.02.025.
[38] A. Brunk, B. Dünweg, H. Egger, O. Habrich, M. Lukáčová-Medvid'Ová, D. Spiller, Analysis of a viscoelastic phase separation model, J. Phys. Condens. Matter 33 (2021) 234002, https://doi.org/10.1088/1361-648X/abeb13.
[39] P. Shen, A. Moriya, S. Rajabzadeh, T. Maruyama, H. Matsuyama, Improvement of the antifouling properties of poly (lactic acid) hollow fiber membranes with poly (lactic acid)-polyethylene glycol-poly (lactic acid) copolymers, Desalination 325 (2013) 37–39, https://doi.org/10.1016/j.desal.2013.06.012.
[40] F. Membrane, K. Keawsupsak, A. Jaiyu, J. Pannoi, P. Somwongsa, N. Wanthausk, P. Sueprasita, Poly (lactic acid)/biodegradable polymer blend for the preparation of flat-sheet membrane, J. Teknol. (Sci. Eng.) 69 (2014) 99–102, https://doi.org/10.11113/jt.v69.3405.
[41] F. De Santis, G. Gorrasi, R. Pantani, A spectroscopic approach to assess transport properties of water vapor in PLA, Polym. Test. 44 (2015) 15–22, https://doi.org/10.1016/j.polymertesting.2015.03.015.
[42] C. Xu, L. Zhang, X. Li, Z.Y. Liu, X. Wang, S.Z. Wang, S. Li, S. Li, H.M. Yin, C. Mao, S. Zhang, J. Gao, H. Xu, Record efficiencies of photothermal conversion and PM capturing by poly(lactic acid) meta-membranes with rose petal-inspired architecture towards extreme environmental applications, Sep. Purif. Technol. 380 (2026) 135539, https://doi.org/10.1016/j.seppur.2025.135539.
[43] M.A. Elsawy, K.H. Kim, J.W. Park, A. Deep, Hydrolytic degradation of polylactic acid (PLA) and its composites, Renew. Sustain. Energy Rev. 79 (2017) 1346–1352, https://doi.org/10.1016/j.rser.2017.05.143.
[44] M. Calosi, A. D'Iorio, E. Buratti, R. Cortesi, S. Franco, R. Angelini, M. Bertoldo, Preparation of high-solid PLA waterborne dispersions with PEG-PLA-PEG block copolymer as surfactant and their use as hydrophobic coating on paper, Prog. Org. Coatings 193 (2024) 108541, https://doi.org/10.1016/j.porgcoat.2024.108541.